Journal of Physics: Conference Series

PAPER • **OPEN ACCESS**

Multi-scale performance evaluation of ejector refrigeration systems

To cite this article: Giorgio Besagni *et al* 2021 *J. Phys.: Conf. Ser.* **1868** 012013

View the article online for updates and enhancements.

IOP ebooks™

Bringing together innovative digital publishing with leading authors from the global scientific community.

Start exploring the collection–download the first chapter of every title for free.

This content was downloaded from IP address 131.175.11.155 on 07/07/2021 at 15:18

Multi-scale performance evaluation of ejector refrigeration systems

Giorgio Besagni[1], Lorenzo Croci[1], Nicolò Cristiani[1,2], Fabio Inzoli[2], Gaël Raymond Guédon[2]

[1]Ricerca sul Sistema Energetico - RSE S.p.A., Power System Development Department, via Rubattino 54, 20134 Milano (Italy)
[2]Politecnico di Milano, Department of Energy, via Lambruschini 4a, 20156, Milano (Italy)

giorgio.besagni@rse-web.it

Abstract. Despite the many advantages, ejector refrigeration systems have not been able to penetrate the market because of two prevailing reasons: low coefficient of performance and relevant influence of ejector operation on the performance of the whole system. Indeed, the performance of ejector refrigeration systems depends on the local flow phenomena occurring within the ejector. Thus, improving the performance of ejector refrigeration systems relies on the understanding of the fluid dynamic phenomena at the "*component-scale*" and on integrating such information at the "*system-scale*". This paper contributes to the present discussion regarding the multi-scale modeling of ejector-based systems by proposing an integrated Computational Fluid Dynamic (*CFD*) - Lumped Parameter Model (*LPM*) ejector refrigeration system. In particular, ejector performances have been obtained by a validated *CFD* approach, whereas a LPM approach has modeled the refrigeration cycle. The refrigeration system's performances, for different boundary conditions, have been evaluated, and the effects of the "*local-scale*" on the "*system-scale*" have been commented.

1. Introduction

The ejector device is constituted by a primary nozzle, a suction chamber, a mixing chamber, and a diffuser (Figure 1a). A "*high energy*" primary flow accelerates and expands through the primary nozzle creating a low-pressure region at the nozzle exit; subsequently, the secondary flow is entrained in the mixing chamber because of the vacuum-effect mentioned above and the shear action between the primary and secondary flows. The primary and secondary flows mix within the mixing chamber and are later compressed in the diffuser, converting kinetic energy into static pressure [1]. The triple effect provided by the ejector (viz., entrainment/compression/mixing) makes it suitable to be employed in refrigeration systems (*ERSs* - Figure 1b, the forthcoming nomenclature refers to this figure). *ERSs* seems a promising alternative to the traditional compressor-based technologies due to their reliability, limited maintenance, low initial and operational costs, and no limitation concerning the working fluids [2]. In an *ERS*, the generator employs low-grade heat energy to produce the "*high energy*" primary flow supplied to the ejector inlet (point#1 in Figure 1b), which entrains the low-pressure secondary flow from the evaporator (point#2 in Figure 1b); subsequently, the mixed stream is conveyed to the condenser (point#3 in Figure 1b) where condensation takes place. Finally, the liquid is split: one part is sent back to the generator by a pump (point#6 in Figure 1b), whereas the other one proceeds towards an expansion

Content from this work may be used under the terms of the Creative Commons Attribution 3.0 licence. Any further distribution of this work must maintain attribution to the author(s) and the title of the work, journal citation and DOI.
Published under licence by IOP Publishing Ltd

valve (point#5 in Figure 1b) and is supplied to the evaporator, thus providing the cooling effect. Relying on low-grade energy source as input, *ERSs* may reduce electricity consumption; unfortunately, they suffer from a low coefficient of performance (*COP* - in the range of 0.1 - 0.7 [1]) and a relevant influence of ejector operation on the performance of the whole system. Indeed, ejector refrigeration systems' performance depends on the local flow phenomena occurring within the ejector (ejector is a "*fluid dynamic controlled device*"). Therefore, the ejector performances (viz., the "*component-scale*", i.e., the ratio between the secondary and the primary mass flow rates – the entrainment ratio – as well as the pressure recovery) results from the fluid-dynamics interaction at the "*local-scale*" (viz., boundary layers subject to adverse pressure gradients, shock waves, over-expanded and under-expanded jets, flow separation, recirculation, turbulence mixing, …). For this reason, precise modeling of *COP* values (viz., the "*system-scale*" performances) relies on a complete knowledge of the "*local-scale*" and the "*component-scale*" performances and a multi-scale coupling of such information [3].

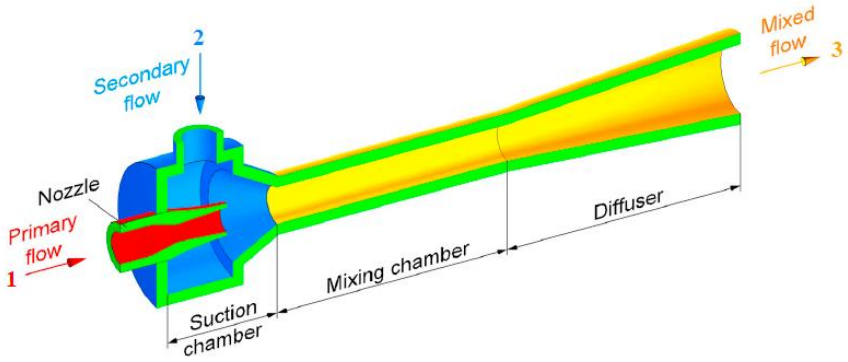

(a) Ejector design

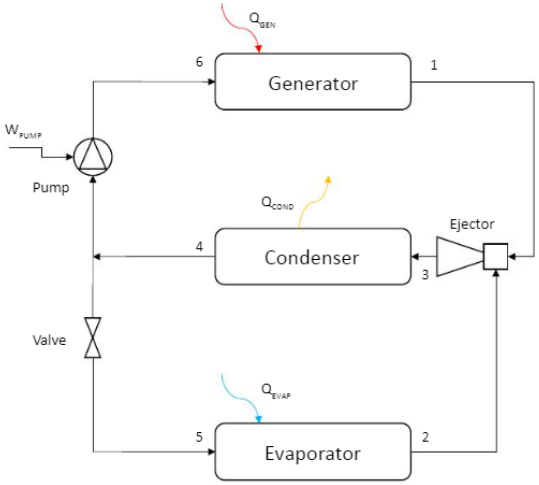

(b) Layout of an ejector refrigeration system (*ERS*)

Figure 1. Ejector component (a) and ejector refrigeration system (b).

In the broader framework of ejector research, this paper contributes to the present-day discussion regarding multi-scale modeling approaches by proposing an integrated Computational Fluid Dynamic (*CFD*) - Lumped Parameter Model (*LPM*) of the ejector refrigeration system. In particular, a validated *CFD* approach solves the fluid-dynamics within the ejector ("*local-scale*") and provides the ejector performances ("*component-scale*"). Conversely, the refrigeration cycle ("*system-scale*") has been modeled by a *LPM* approach using input data CFD outcomes. In conclusion, the proposed model can consider the multi-scale relationships that determine the overall *ERS* performances.

2. Methods: benchmark and numerical modeling

In this section, the integrated Computational Fluid Dynamic (*CFD*) - Lumped Parameter Model (*LPM*) is outlined. First, the numerical validation benchmark is presented; subsequently, *CFD* and *LPM methods* are described.

2.1. Benchmark

The numerical model has been validated against an R134a ejector, described by Del Valle et al. [4], whose geometry and boundary conditions are presented in Figure 2 and Table 1. It should be noted that a constant 10°C superheating for both primary and secondary inlets (included in Table 1) has been prescribed accordingly to the experimental boundary conditions. In this study, both global (ω, the entrainment ratio; viz., the ratio between the secondary and the primary mass flow rate) and local (wall static pressure along with the ejector) measurements are available for complete validation.

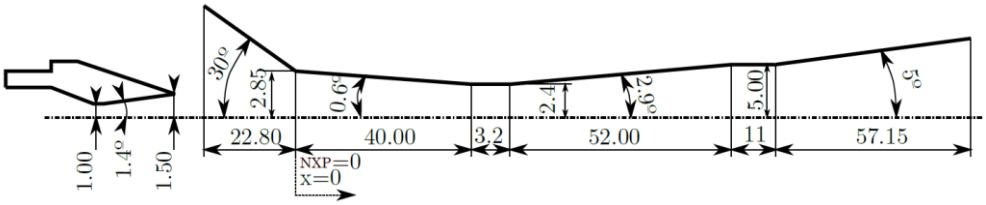

Figure 2. Ejector design from ref. [4]; dimensions in [mm].

Table 1. Boundary conditions for the different validation cases.

Code Name	T_1 [°C]	P_1 [kPa]	T_2 [°C]	P_2 [kPa]	P_3 [kPa]	ω_{Exp}
Case#1	84.2	2,330	20	415	650	0.592
Case#2	100.03	3,190	15	350	690	0.361
Case#3	100.03	3,190	20	415	690	0.433

2.2. Numerical modeling

The finite volume code ANSYS Fluent (*Release 2020 – R1*) has been used to solve the steady-state Reynolds Averaged Navier-Stokes (*RANS*) equations for the turbulent compressible Newtonian flow, employing *k-ω* SST as turbulence model (as discussed in ref. [3]). A two-dimensional axisymmetric calculation has been performed. To limit the numerical diffusion, second-order upwind numerical schemes have been used for the spatial discretization, except for the pressure equation. In this case, PRESTO! scheme has been chosen since it is designed for flows involving steep pressure gradients. Second-order upwind schemes also for the turbulence model variables have been used. Gradients are evaluated by a least-squares approach. A two-step approach has performed the initialization: (i) a hybrid initialization followed by a (ii) full multi-grid (*FMG*) scheme. A pressure-based solver with a Coupled algorithm has been adopted since it is described by Croquer et al. [5] as far more stable than density based-solver nevertheless sufficiently accurate and suitable for high-velocity compressible flows. A pseudo-transient option was enabled, which was found to speed up the steady-state solution. R134a properties have been evaluated with the real-gas NIST database; indeed, Del Valle et al. [4] mentioned that the implementation of a real gas model is needed to correctly model non-ideal fluid phenomena under the refrigeration system boundary conditions. Ejector inlet boundary conditions are prescribed in terms of total pressure and temperature, while the turbulence boundary conditions have been implemented as hydraulic diameter and the turbulent intensity (5% for the primary flows and 2% for the second one) as described by Besagni and Inzoli [3]. The outlet condition has been modeled as a pressure boundary condition.

2.3. Multi-scale modeling

The above-described *CFD* model is used to solve the "*component-scale*" (viz., the entrainment ratio ω) and the fluid-dynamics ("*local-scale*") of the tested ejector. Once such information is derived, the ejector component is then included within *ERS*, modeled by a *LPM* approach, to estimate the "*system-scale*"

performances. The advantage of such an approach is to take into account the fluid dynamics phenomena within the cycle performances. In particular, *LPM* input data concern (i) P_1, T_1 (comprehending a 10°C superheating indicated as ΔT_{sh}), P_2, T_2 (comprehending a 10°C superheating indicated as ΔT_{sh}) and P_3 (Figure 1a), which act as boundary conditions for the *CFD* simulations and (ii) the mass flow rates $\dot{m}_1$ and $\dot{m}_2$ and T_3, which are the *CFD* model output. To model *ERS*, the prevailing assumption concerns the absence of pressure losses within the system so to relate ejector boundary conditions to the cycle pressure and temperature levels (Figure 1b). The *LPM* approach is presented in the forthcoming equations, where sub-scripts *gen* stands for generator, *evap* for the evaporator while *cond* for the condenser. The saturated vapor is indicated by subscript *sv*, while saturated liquid by *sl*. Finally, apex *is* stands for isentropic. First, pressure values are computed as follows:

$$P_1=P_6=P_{gen} \quad (1)$$
$$P_2=P_5=P_{evap} \quad (2)$$
$$P_3=P_4=P_{cond} \quad (3)$$

Based on the *CFD* boundary conditions, points#1 and #2 (Figure 1b) are characterized as follows:

$$T_1= T_{sv}(P_1) + \Delta T_{sh} \quad (4)$$
$$h_1= h(P_1,T_1) \quad (5)$$
$$s_1=s(P_1,T_1) \quad (6)$$
$$T_2= T_{sv}(P_2) + \Delta T_{sh} \quad (7)$$
$$h_2= h(P_2,T_2) \quad (8)$$
$$s_2=s(P_2,T_2) \quad (9)$$

Point #3 (Figure 1b) is computed from *CFD* outcomes as ejector outlet temperature (T_3) results from the mixing of primary and secondary streams.

$$h_3= h(P_3,T_3) \quad (10)$$
$$s_3=s(P_3,T_3) \quad (11)$$

Point#4 (Figure 1b) is computed based on a saturated liquid assumption:

$$P_4=P_{cond} \quad (12)$$
$$T_4=T_{cond} \quad (13)$$
$$h_4=h_{sl}(P_{cond}) \quad (14)$$
$$s_4=s_{sl}(P_{cond}) \quad (15)$$

Point#5 (Figure 1b) is computed considering an isenthalpic transformation in the expansion valve:

$$h_5=h_4 \quad (16)$$
$$T_5=T_{evap} \quad (17)$$
$$s_5=s(P_5,h_5) \quad (18)$$

Point#6 (Figure 1b) is computed assuming the isentropic efficiency of the pump η^{is}_{pump} = 0.9 [6]:

$$h_6^{is}=h(P_6,s_4) \quad (19)$$
$$h_6=h_4+\frac{h_6^{is}-h_4}{\eta^{is}_{pump}} \quad (20)$$
$$T_6=T(P_6,h_6) \quad (21)$$
$$s_6=s(P_6,h_6) \quad (22)$$

After all thermodynamic points of the *ERS* cycle are defined, the cooling power ($\dot{Q}_{evap}$), input thermal power ($\dot{Q}_{gen}$) and electrical power required by the pump ($\dot{W}_{pump}$) are computed using as input the mass flow rates $\dot{m}_1$ and $\dot{m}_2$, which are *CFD* model output:

$$\dot{Q}_{evap}=\dot{m}_2(h_2-h_5) \quad (23)$$

$$\dot{Q}_{gen}=\dot{m}_1(h_1-h_6) \quad (24)$$

$$\dot{W}_{pump}=\dot{m}_1(h_6-h_4) \quad (25)$$

Finally, cycle *COP* is computed as follows:

$$COP=\frac{\dot{Q}_{evap}}{\dot{Q}_{gen}+\dot{W}_{pump}}=\omega\frac{h_2-h_5}{h_1-h_4} \quad (26)$$

3. Results

This section presents and discusses the numerical results. First, the *CFD* approach is validated against experimental data; subsequently, *CFD* outcomes are coupled to the *LPM* approach.

3.1. Validation and local-scale fluid dynamics

The *CFD* approach has been validated considering both global (*ω,* the entrainment ratio) and local (wall static pressure profiles) quantities. Indeed, as stated by Hemidi et al. [7], a validation based upon "*component-scale*" data only may be misleading as the same entrainment ratio could emerge from different local flow structures. From a practical point of view, *CFD* and experimental data are compared based on (i) the entrainment ratio relative error (Equation (29)) and (ii) the mean absolute error between computed and experimental wall static pressure data (Equation (30)).

$$\text{Relative error} = \frac{\omega_{CFD} - \omega_{EXP}}{\omega_{EXP}} \quad (27)$$

$$\text{Mean absolute error} = \sum\left[\frac{|P_{CFD} - P_{EXP}|}{P_{EXP}}/n\right] \quad (28)$$

Where *n* is the number of data points. The validation procedure outcome is summarized in Table 2, whereas Figure 3 displays wall pressure profiles. *CFD* outcomes show a fair agreement compared with the experimental data: entrainment ratios have been predicted with a maximum relative error equal to 17.4%, whereas the mean absolute error for the local pressure profiles is lower than 10%. It is worth noting that the *CFD* approach has been able to correctly predict the sudden pressure drop within the mixing chamber, as well as the pressure rise caused by the shockwave at the diffuser inlet.

Table 2. *CFD* model validation results for the tested cases (Table 1).

Code Name	ω_{Exp}	ω_{CFD}	Relative error [%]	Mean absolute error [%]
Case#1	0.592	0.695	17.4%	4.80%
Case#2	0.361	0.421	16.6%	7.95%
Case#3	0.433	0.495	14.3%	9.13%

3.2. ERS performances and multi-scale perspective

ERS performances have been computed based on the modeling approach described in Section 2.3. It is worth noting that *COP* is related to ω (Equation (28)), thus linking ejector and system performances. The outcome of the *ERS* performances, in terms of *COP* and cooling power, are listed in Table 3, whereas the details of the different cases are displayed in Figure 4, Figure 5, and Figure 6.

Table 3. *ERS* performances for the tested cases (Table 1).

Code Name	ω [-]	*COP* [-]	$\dot{Q}_{evap}$ [kW]
Case#1	0.695	0.594	3.76
Case#2	0.421	0.345	3.05
Case#3	0.495	0.413	3.65

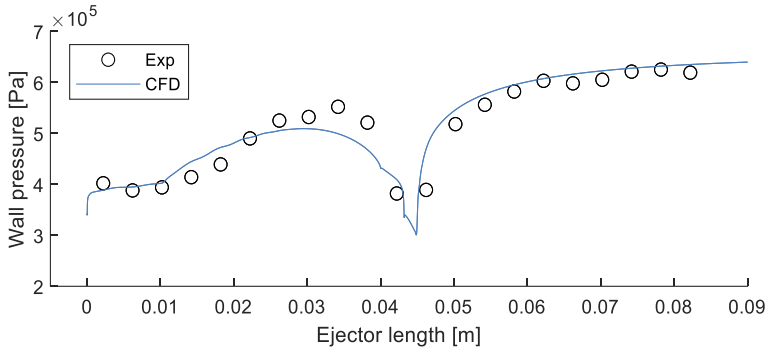

(a) Case#1 (T_1 = 84.2°C, P_1 = 2,330 kPa, T_2 = 20.0°C, P_2 = 415 kPa, P_3 = 650 kPa)

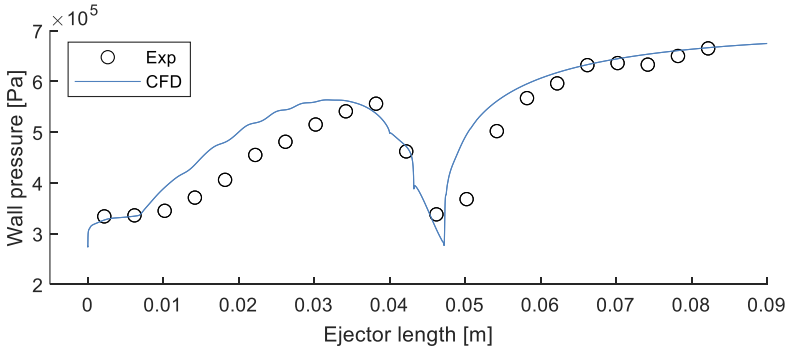

(b) Case#2 (T_1 = 100.0°C, P_1 = 3,190 kPa, T_2 = 15.0°C, P_2 = 350 kPa, P_3 = 690 kPa)

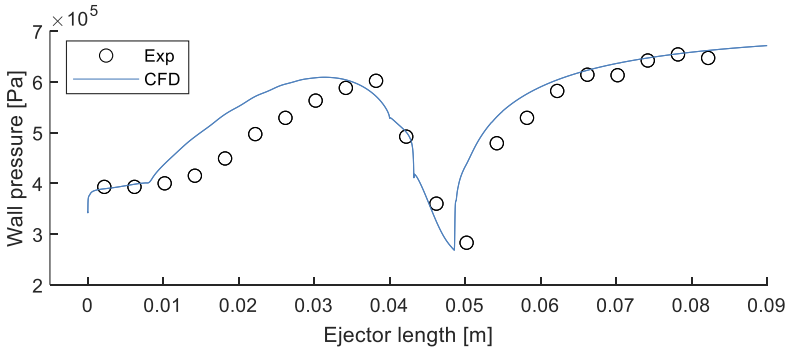

(c) Case#3 (T_1 = 100.0°C, P_1 = 3,190 k Pa, T_2 = 20.0°C, P_2 = 415 kPa, P_3 = 690 kPa)

Figure 3. Wall pressure profiles for the tested cases (Table 1).

It is noted that the highest cycle performance (COP = 0.594) has been obtained with Case#1, which is characterized by the lowest T_1 (see the boundary conditions in Table 1). Comparing Case#2 and Case #3, the latter has higher COP, owing to the higher P_2. It is worth noting that *CFD* capability to solve the local flow phenomena (the "*local-scale*") allows us to understand the prevailing reasons behind these observations. In particular, the primary jet's expansion affects the available cross-section area to entrain the secondary flow (the so-called entrainment duct). An increase in T_1 (viz., P_1, as the superheating has been kept constant and equal to 10°C for all the three tested cases) promotes the primary flow expansion, thus resulting in the reduction of the available cross-section area to entrain the secondary flow, with the consequent decrease of ω and thus COP, in agreement with ref. [8]. Higher P_1, on the other hand, would result in a higher critical pressure (viz., the outlet pressure for which ejector changes from on-design to off-design operation mode, causing a rapid decrease of ω [1]), extending the ejector operating curve. Increasing T_2 reduces the primary flow expansion and, for fixed primary flow conditions, it improves ω and COP: this is made clear by comparing Case#2 and Case#3 (ω increased by 17.6%, COP increased by 19.7%).

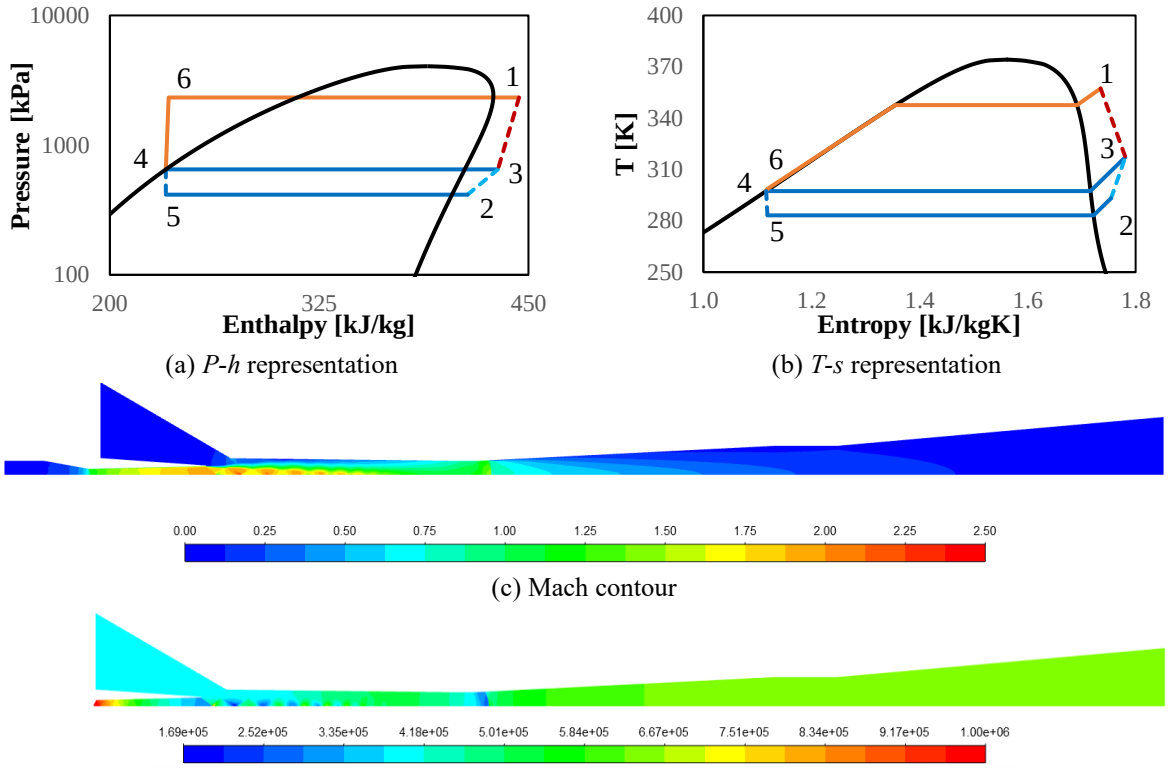

(a) *P-h* representation (b) *T-s* representation

(c) Mach contour

(d) Pressure contour

Figure 4. Case#1 (T_1 = 84.2°C, P_1 = 2,330 kPa, T_2 = 20.0°C, P_2 = 415 kPa, P_3 = 650 kPa).

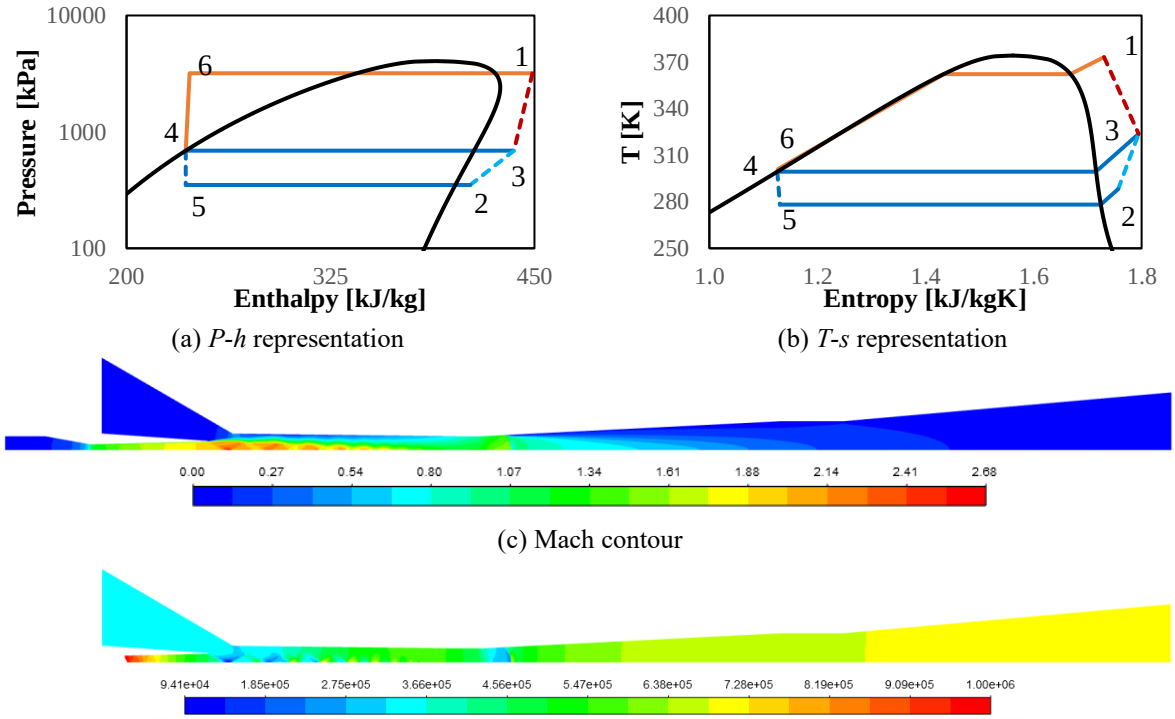

(a) *P-h* representation (b) *T-s* representation

(c) Mach contour

(d) Pressure contour

Figure 5. Case#2 (T_1 = 100.0°C, P_1 = 3,190 kPa, T_2 = 15.0°C, P_2 = 350 kPa, P_3 = 690 kPa).

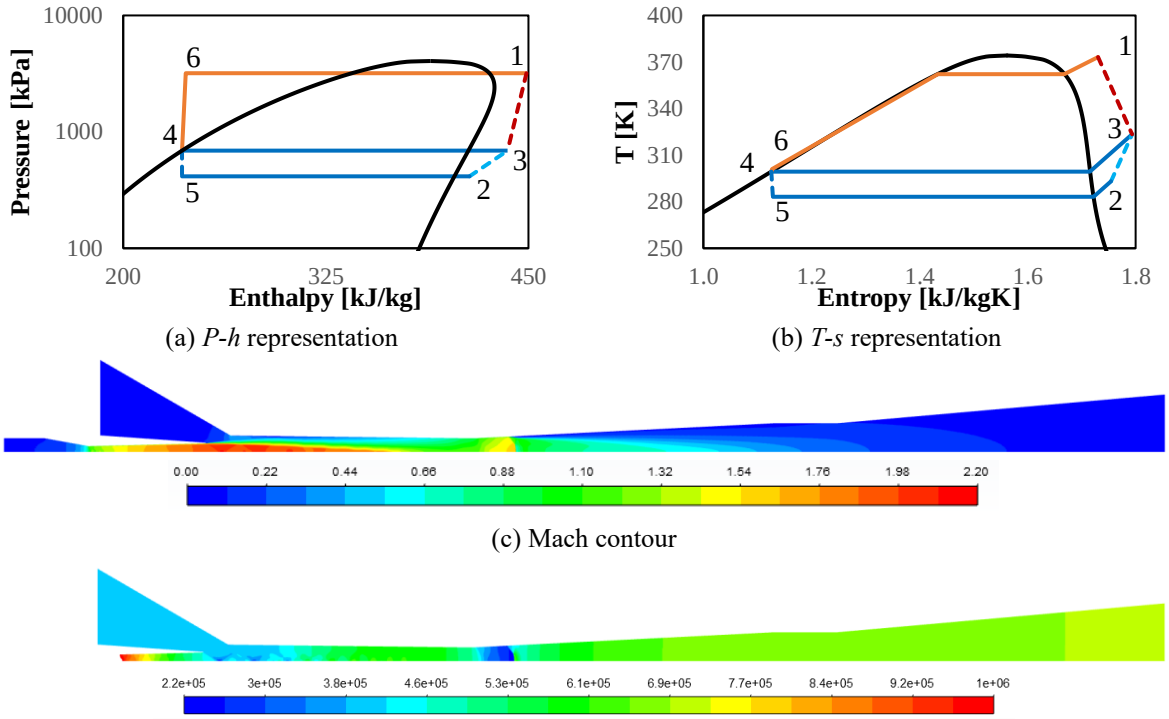

(a) *P-h* representation (b) *T-s* representation

(c) Mach contour

(d) Pressure contour

Figure 6. Case#3 (T_1 = 100.0°C, P_1 = 3,190 kPa, T_2 = 20.0°C, P_2 = 415 kPa, P_3 = 690 kPa).

4. Conclusions

A multi-scale integrated Computational Fluid Dynamic (*CFD*) - Lumped Parameter Model (*LPM*) of the *ERS* has been presented. The integrated model relies on a *CFD* approach to solve the ejector fluid-dynamics (viz., the "*local-scale*") and the ejector performance (viz., the "*component-scale*"). Conversely, the *ERS* system is instead modeled by an *LPM* that evaluates the cycle performances (viz., the "*system-scale*") based on *CFD* outcomes. The advantage of such an approach is to relate the "*local-scale*" to the "*system-scale*", which has been proved by the herein application of the proposed multi-scale model to a R134a driven ejector.

5. Acknowledgments

This work has been financed by the Research Fund for the Italian Electrical System in compliance with the Decree of Minister of Economic Development April 16, 2018.

6. References

[1] Aidoun Z, Ameur K, Falsafioon M and Badache M 2019 *Inventions* **4** 15
[2] Besagni G, Mereu R and Inzoli F 2016 *Renew. Sust. Energ. Rev.* **53** 373-407
[3] Besagni G and Inzoli F 2017 *Appl. Therm. Eng.* **117** 122-44
[4] García Del Valle J, Sierra-Pallares J, Garcia Carrascal P and Castro Ruiz F 2015 *Appl. Therm. Eng.* **89** 795-811
[5] Croquer S, Poncet S and Aidoun Z 2016 *Int. J. Refrig.* **61** 140-52
[6] Fang Y, Croquer S, Poncet S, Aidoun Z and Bartosiewicz Y 2017 *Int. J. Refrig.* **77** 87-98
[7] Hemidi A, Henry F, Leclaire S, Seynhaeve J M and Bartosiewicz Y *Appl. Therm. Eng.* 2009 **29** 1523-31
[8] Chunnanond K and Aphornratana S 2004 *Appl. Therm. Eng* **24** 311-22